Research Article | Vol. 25, No. 23 | 13 Nov 2017 | OPTICS EXPRESS 28427
Optics EXPRESS

Automatic real-time focus control system for laser processing using dynamic focusing optical system

Binh Xuan Cao,[1,2] Phuong Hoang Le,[3] Sanghoon Ahn,[1] Heeshin Kang,[1] Jengo Kim,[1] and Jiwhan Noh[1,2,*]

[1]*Department of Laser and Electron Beam Application, Korea Institute of Machinery & Materials (KIMM), Daejeon 34103, South Korea*
[2]*Department of Nano-Mechatronics, Korea University of Science and Technology (UST), Daejeon 34113, South Korea*
[3]*Department of Material Science and Engineering, Korea Advanced Institute of Science and Technology (KAIST), Daejeon 34141, South Korea*
[*]*njw733@kimm.re.kr*

Abstract: An automatic real-time focus inspection system based on a combination of dynamic focusing and real-time focus detection is introduced for use in high-precision laser processing. The system allows for accurately and rapidly positioning the laser focus on the target surface, wherever it is located along the optical axis. The proposed method is superior to conventional methods because it not only offers accurate, versatile, and high-speed autofocusing, but also combines well with the fabrication laser to perform laser processing when the laser focus is located on the sample. In this system, the laser focus is flexibly and automatically shifted along the optical axis by a dynamic focusing device to rapidly meet the working surface, ensuring high quality and complexity of fabricated patterns. Thus, the laser focus is not restricted to the focal point of the objective lens of infinity corrected microscopes reported previously. Furthermore, the focal spot analytically maintains its size with a size deviation less than 0.1% while the focus is slightly shifted along the optical axis, guaranteeing the size and quality of fabricated patterns. The proposed method is expected to lead to a high-precision laser fabrication system that can be widely applied in both science and the industry.

OCIS codes: (120.0120) Instrumentation, measurement, and metrology; (140.3390) Laser materials processing; (220.4610) Optical fabrication; (220.3620) Lens system design.

References and links

1. G. B. J. Cadot, D. A. Axinte, and J. Billingham, "Continuous trench, pulsed laser ablation for micro-machining applications," Int. J. Mach. Tools Manuf. **107**, 8–20 (2016).
2. Z. Hao, J. Wang, P. Yao, and C. Huang, "Heat transfer and material ablation in hybrid laser-waterjet microgrooving of single crystalline germanium," Int. J. Mach. Tools Manuf. **116**, 25–39 (2017).
3. C. Chen, M. Gao, and X. Zeng, "Relationship between temperature at cut front edge and kerf quality in fiber laser cutting of Al–Cu aluminum alloy," Int. J. Mach. Tools Manuf. **109**, 58–64 (2016).
4. Y. Ito, T. Kizaki, R. Shinomoto, M. Ueki, N. Sugita, and M. Mitsuishi, "High-efficiency and precision cutting of glass by selective laser-assisted milling," Precis. Eng. **47**, 498–507 (2017).
5. S. Mullick, Y. K. Madhukar, S. Roy, and A. K. Nath, "An investigation of energy loss mechanisms in water-jet assisted underwater laser cutting process using an analytical model," Int. J. Mach. Tools Manuf. **91**, 62–75 (2015).
6. I. Karnadi, J. Son, J.-Y. Kim, H. Jang, S. Lee, K. S. Kim, B. Min, and Y.-H. Lee, "A printed nanobeam laser on a SiO2/Si substrate for low-threshold continuous-wave operation," Opt. Express **22**(10), 12115–12121 (2014).
7. T. Ishigure, K. Shitanda, and Y. Oizmi, "Index-profile design for low-loss crossed multimode waveguide for optical printed circuit board," Opt. Express **23**(17), 22262–22273 (2015).
8. S. Feng, C. Qin, K. Shang, S. Pathak, W. Lai, B. Guan, M. Clements, T. Su, G. Liu, H. Lu, R. P. Scott, and S. J. Ben Yoo, "Rapidly reconfigurable high-fidelity optical arbitrary waveform generation in heterogeneous photonic integrated circuits," Opt. Express **25**(8), 8872–8885 (2017).
9. J. Houzet, N. Faure, M. Larochette, A.-C. Brulez, S. Benayoun, and C. Mauclair, "Ultrafast laser spatial beam shaping based on Zernike polynomials for surface processing," Opt. Express **24**(6), 6542–6552 (2016).

#307503 https://doi.org/10.1364/OE.25.028427
Journal © 2017 Received 20 Sep 2017; revised 24 Oct 2017; accepted 25 Oct 2017; published 1 Nov 2017

Optics EXPRESS

10. K.-C. Fan, C.-L. Chu, and J.-I. Mou, "Development of a low-cost focusing probe for profile measurement," Meas. Sci. Technol. **12**, 2137–2146 (2001).
11. H.-G. Rhee, D.-I. Kim, and Y.-W. Lee, "Realization and performance evaluation of high speed autofocusing for direct laser lithography," Rev. Sci. Instrum. **80**(7), 073103 (2009).
12. J. Luo, Y. Liang, and G. Yang, "Realization of autofocusing system for laser direct writing on non-planar surfaces," Rev. Sci. Instrum. **83**(5), 053102 (2012).
13. B. X. Cao, P. Le Hoang, S. Ahn, J. O. Kim, and J. Noh, "High-precision detection of focal position on a curved surface for laser processing," Precis. Eng. **50**, 204–210 (2017).
14. B. J. Jung, H. J. Kong, B. G. Jeon, D. Y. Yang, Y. Son, and K. S. Lee, "Autofocusing method using fluorescence detection for precise two-photon nanofabrication," Opt. Express **19**(23), 22659–22668 (2011).
15. M. Antti, H. Ville, and V. Jorma, "Precise online auto-focus system in high speed laser micromachining applications," Phys. Procedia **39**, 807–813 (2012).
16. O. Armbruster, A. Naghilou, H. Pöhl, and W. Kautek, "In-situ and non-destructive focus determination device for high precision laser applications," J. Opt. **18**, 095401 (2016).
17. B. X. Cao, M. Bae, H. Sohn, J. Choi, Y. Kim, J.-O. Kim, and J. Noh, "Design and performance of a focus-detection system for use in laser micromachining," Micromachines (Basel) **7**(1), 2 (2016).
18. B. X. Cao, P. Hoang, S. Ahn, J.-O. Kim, H. Sohn, and J. Noh, "Real-time detection of focal position of workpiece surface during laser processing using diffractive beam samplers," Opt. Lasers Eng. **86**, 92–97 (2016).
19. D. Wang, X. Ding, T. Zhang, and H. Kuang, "A fast auto-focusing technique for the long focal lens TDI CCD camera in remote sensing applications," Opt. Laser Technol. **45**, 190–197 (2012).
20. I. A. Martínez and D. Petrov, "Back-focal-plane position detection with extended linear range for photonic force microscopy," Appl. Opt. **51**(25), 5973–5977 (2012).
21. P. Annibale, A. Dvornikov, and E. Gratton, "Optical measurement of focal offset in tunable lenses," Opt. Express **24**(2), 1031–1036 (2016).
22. I. Alexeev, J. Strauss, A. Gröschl, K. Cvecek, and M. Schmidt, "Laser focus positioning method with submicrometer accuracy," Appl. Opt. **52**(3), 415–421 (2013).
23. W.-Y. Hsu, C. S. Lee, P. J. Chen, N. T. Chen, F. Z. Chen, Z. R. Yu, C. H. Kuo, and C. H. Hwang, "Development of the fast astigmatic auto-focus microscope system," Meas. Sci. Technol. **20**, 045902 (2009).
24. C.-S. Liu, P.-H. Hu, and Y.-C. Lin, "Design and experimental validation of novel optics-based autofocusing microscope," Appl. Phys. B **109**, 259 (2012).
25. C.-S. Liu, Y.-C. Lin, and P.-H. Hu, "Design and characterization of precise laser-based autofocusing microscope with reduced geometrical fluctuations," Microsyst. Technol. **19**, 1717–1724 (2013).
26. C.-S. Liu and S.-H. Jiang, "Design and experimental validation of novel enhanced-performance autofocusing microscope," Appl. Phys. B **117**, 1161 (2014).
27. C.-S. Liu, Z.-Y. Wang, and Y.-C. Chang, "Design and characterization of high-performance autofocusing microscope with zoom in/out functions," Appl. Phys. B **121**, 69 (2015).
28. C.-S. Liu and S.-H. Jiang, "Precise autofocusing microscope with rapid response," Opt. Lasers Eng. **66**, 294–300 (2015).
29. A. Weiss, A. Obotnine, and A. Lasinski, "Method and apparatus for the auto-focusing infinity corrected microscopes," U.S. Patent 7700903 B2 (2010).
30. B. X. Cao, P. L. Hoang, S. Ahn, J.-O. Kim, H. Kang, and J. Noh, "In-situ real-time focus detection during laser processing using double-hole masks and advanced image sensor software," Sensors (Basel) **17**(7), 1540 (2017).

1. Introduction

The optical energy of laser beams with high intensity, proper orientation, and simple manipulation is employed to perform several tasks of laser processing that require high precision, such as ablation [1,2], cutting [3–5], circuit printing [6–8], and micro-grooving [9]. However, the out-of-focus state of the laser at the target surface during laser processing poses tremendous disadvantages in both scientific and industrial applications. In laser processing, imperfect focusing produces micro-patterns with low quality and defects on the surface. Therefore, the creation of an automatic focus inspection system for precisely positioning the laser focus on the working surface during processing has become increasingly significant and urgent because precision, sophistication, and productivity are prerequisites for products of laser processing as well as laser micro-printing.

Several papers and technical schemes have reported novel techniques for high-precision, high-speed laser focus inspection in different conditions, which are applied in a wide range of industrial and scientific applications [10–20]. A good focusing condition plays an important role in profile measurement [10], increasing the productivity of modern patterning methods such as direct laser lithography on non-planar surfaces [11–13], two-photon nano-fabrication [14], laser micromachining using a charge-coupled device (CCD) camera and testing of the

Optics EXPRESS

performance of laser fabrication at the focal position as well as defocus positions with various laser powers and diffractive beam samplers [15–18], remote sensing using time delay and integration (TDI) CCD cameras [19], and photonic force microscopy [20]. In addition, some other focus positioning methods have been proposed without specific applicability in technology or the industry [21–23], such as focal offset inspection [21], workpiece position determination [22], and four-quadrant photodiode utilization [23], for cases with a short working range.

Several papers by C. S. Liu have focused on the technique of using a bisected laser beam for autofocusing a microscope [24–28], but this technique has several limitations. The system used a bisected laser beam to detect the focal position with a combination of two achromatic lenses [24,25], two cylindrical lens assemblies [26], a tunable optical zoom system [27], and a high-speed optical rotating diffuser [28]. However, this method is not applicable to laser processing, because the system is not well integrated with high-intensity fabrication lasers, even though the principle of the focus inspection method is well defined. Moreover, the detection range demonstrated in these papers is restricted from –200 μ m to 200 μ m, which is considered narrow in laser technology and is smaller than that of the newest focus inspection device established by Metrology Sensors GmbH (MSG) [29]. The most recently proposed system for in situ real-time focus detection using two laser sources during laser fabrication was designed with a double-hole mask and an advanced image sensor, which replaced the conventional CCD camera for higher resolution and accuracy [30]. These systems all play significant roles in the enhancement of focus detection systems. However, while previous methods can only detect the focus and adjust the target surface on the detected point, an automatic real-time focus control system that maintains the on-focus status of the target surface throughout the laser processing period remains a challenging goal, which we have attempted to achieve.

In this paper, an automatic real-time focus control system with a combination of a focus detection system using an advanced image sensor and a dynamic focusing system is presented. The system automatically and precisely moves and locates the fabrication laser focus onto the target surface during laser processing in real time to fabricate micro-holes with a size variation of approximately 0.1 nm. With the achievements of previous in situ real-time focus detection systems, the proposed method guarantees reproducibility and flexibility when fabricating a huge number of target samples without resetting the fabrication system during pattern production; thus, our method is superior to conventional methods. The present article will recall the design and operation of the double-spot focus detection system using an advanced image sensor, introduce the dynamic focusing system that can shift the fabrication laser focus according to the position of the sample surface by moving a componential negative lens, and present the method of integration between double-spot focus detection and dynamic focusing systems. Subsequently, an experimental analysis of the method is presented, and the theoretical model and experimental result are shown to be consistent. The technique marks a significant milestone for laser processing in particular and focus control in general, contributing to the increase of the productivity, precision, and flexibility of micro-groove processing on stepped surfaces using high-intensity ultrafast lasers as well as auto-focusing optical microscopes.

Optics EXPRESS

2. Dynamic focusing optical system for high-precision focus imaging

2.1 Description of dynamic focusing system

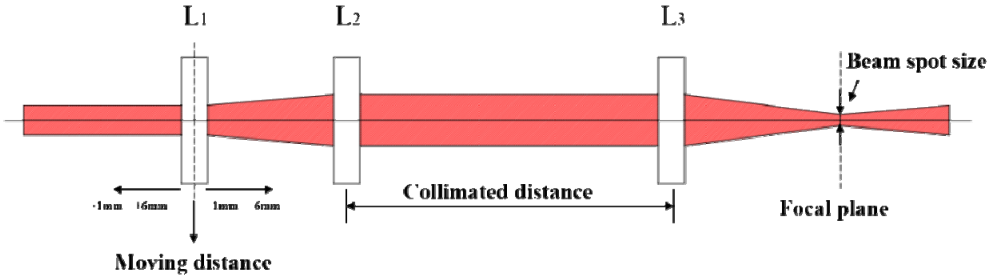

Fig. 1. Schematic of the dynamic focusing optical system for shifting the fabrication laser focus.

The system consists of a moveable negative lens L_1 with focal length f_1 and a stable positive lens L_2 with focal length f_2. In this system, the position of lens L_2 is fixed, while lens L_1 is moveable. Initially, two lenses are properly arranged such that an incident collimated laser beam passing through the system becomes collimated with a larger aperture, as shown in Fig. 1. The distance between the positive lens and objective lens is the collimated distance. The collimated beam then passes through an objective lens OL (L_3) with focal length f and is focused on the focal plane of this lens, which is at a distance f from the objective lens on the image sensor. This position of the image sensor is called the zero point. When the negative lens L_1 is moved away from the initial position, the outgoing laser beam from the dynamic focusing system is no longer collimated but is rather focused on a plane between the planes of lenses L_2 and L_3. Consequently, the beam finally focuses on another plane of the image sensor, which is not the focal plane of the objective lens f. Thus, the image sensor is shifted away from the zero point to catch the laser focal spot. As the lens L_1 is shifted around the initial point, the laser focal point is moved around the zero point, which is defined as the initial focal position. The purpose of this system is to precisely focus on a target sample surface with arbitrary roughness during processing, such as micro-groove processing on a stepped surface with high intensity laser.

Table 1. Change in focal position and fabrication laser beam spot size as the negative lens is shifted around the initial point

Moving distance of Lens L_2 (mm)	Image sensor position (mm)	Distance gap (mm)	Beam spot size at focus (μm)
–6	9.1	–7.29	1.359988128
–5	10.21	–6.18	1.359967019
–4	11.7	–4.69	1.359994581
–3	12.22	–4.17	1.359992733
–2	13.7	–2.69	1.359989036
–1	15.4	–0.99	1.359977925
0	16.39	0	1.359999933
+ 1	17.56	+ 1.17	1.360022344
+ 2	18.85	+ 2.46	1.360011231
+ 3	20.54	+ 4.15	1.360007533
+ 4	21.46	+ 5.07	1.360005686
+ 5	23.6	+ 7.21	1.360004579
+ 6	24.39	+ 8	1.360003841

Optics EXPRESS

The optical apparatus for investigating the relation between the displacements of the negative lens and the focus includes the dynamic focusing system, an objective lens (M Plan Apo NIR 5x, Mitoyo, Japan), and a titled u-Nova20M image sensor (1600 × 1200, 50 fps, Mono, Global Shutter, CMOS). The diode laser beam passes through L_1 of focal length −50 mm, L_2 of focal length 100 mm, and OL of focal length 140 mm, and is incident on the image sensor. Considering the experimental procedure, initially, the image sensor is at the zero point or initial focal position at which the beam spot is the smallest with respect to the initial position of the negative lens. The negative lens is shifted around the initial position with tunable increments of 1 mm in the range from −6 to 6 mm while other optical elements are kept stable. For each position of the negative lens, the image sensor is shifted by a micro-positioning stage along the optical axis until the smallest beam spot is recorded, and the corresponding position of the image sensor is recorded simultaneously. Table 1 indicates the variation of the laser focus position (or image sensor) and the beam spot size at the focal position with respect to the zero point due to the movement of the negative lens L_1 with respect to the initial point. In the table, the first column indicates the movement of the negative lens according to the focal-position displacement, which is expressed by the movement of the image sensor in the second column. The third column of the table indicates the distance between each position of the image sensor according to the position of L_1 and the initial focal position. From this table, the relation between the focal position of the fabrication laser and the position of the negative lens can be sketched. The function of the system is the automatic control of laser focus by shifting the negative lens L_1. The fourth column's data indicate the changes in focal spot size with respect to the position of negative lens L_1. The fabrication beam spot size obtained by the image sensor is slightly varied around 1.36 μm (Table 1) with a deviation less than 1 nm (0.1%) while the lens L_1 is shifted in the range from −6 to 6 mm around the initial position with tunable increments of 0.1 mm. The following part of this section will analyze the relation between the position of the laser focal point and the position of the negative lens inside the dynamic focusing system on the basis of beam optics.

Optics EXPRESS

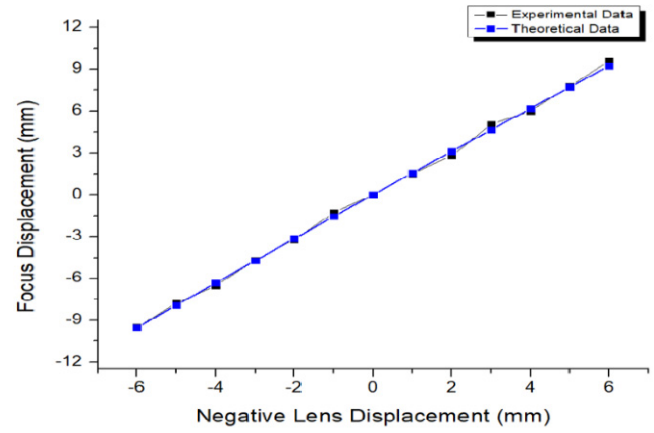

(a)

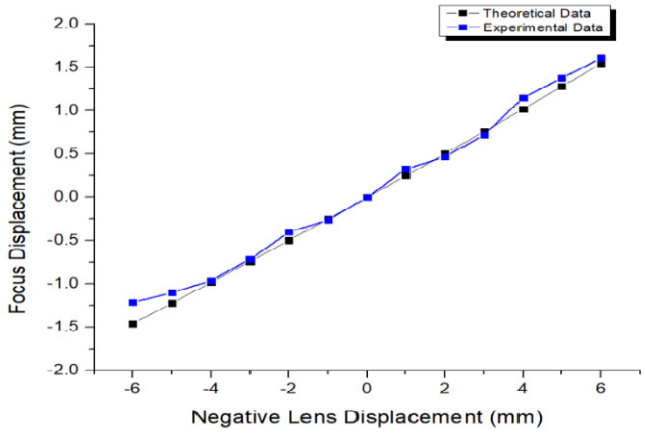

(b)

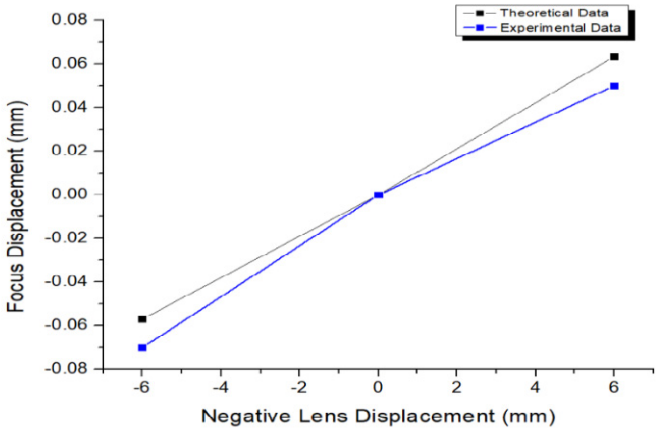

(c)

Fig. 2. Relation between the position of laser focus and position of negative lens for different objective lenses. (a) Objective focal length of 125 mm. (b) Objective focal length of 50 mm. (c) Objective focal length of 10 mm.

Optics EXPRESS

The inspection of the focus-controlling capability and flexibility of the dynamic focusing system with objective lenses of different focal lengths is crucial for satisfying laser fabrication on a sample with arbitrary roughness. For this purpose, we perform the experiment mentioned above with lenses of focal lengths 125 mm, 50 mm, 10 mm to sketch the corresponding relations between the movement of the negative lens and of the laser focal position. Graphs including experimental and simulation data are shown in Fig. 2, in which the horizontal axis indicates the movement of the negative lens and the vertical axis indicates the acquired shifting of laser focus. The experimental and simulation data are remarkably consistent. It can be seen from the result that, when the focal length of the objective lens increases, the slope of the relation increases accordingly. This means that a small deviation of the negative lens leads to a large displacement of the focus. Eventually, a better resolution of measurement is attained by the larger focal length of the objective lens.

2.2 Analytical model

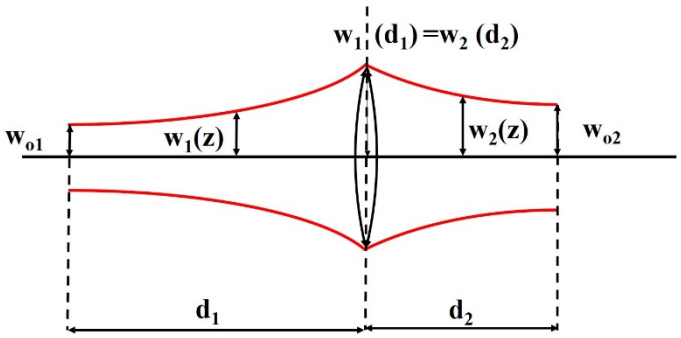

Fig. 3. Transmission of a Gaussian beam through a thin lens [18].

First, we describe a simple model in which a diverged beam passes through a thin lens and converges behind the lens. Consider a beam waist w_{o1} as an object with a thin lens having a focal length f located at a distance d_1 away from it along the beam axis. The obtained image is located at a distance d_2 away from the lens with a beam waist w_{o2}, as shown in Fig. 3. Furthermore, according to the definitions of the beam width and the radius of curvature of the wavefronts comprising the beam [18], the beam width can be expressed as follows:

$$w(z) = w_o\sqrt{1+\left(\frac{z}{z_R}\right)^2}. \tag{1}$$

Where $w(z)$ is either $w_1(z)$ or $w_2(z)$, w_o is either w_{o1} or w_{o2}, and $z_R = \frac{\pi w_o^2}{\lambda}$ is the Rayleigh range.

According to [18], we can obtain with $\frac{\pi w_{o1}^2}{\lambda f} \ll 1$:

$$\frac{d_2}{f} = 1+\frac{\frac{d_1}{f}-1}{\left(\frac{d_1}{f}-1\right)^2+\left(\frac{\pi w_{o1}^2}{\lambda f}\right)^2} \approx \frac{d_1}{d_1-f} \rightarrow d_2 = \frac{d_1 f}{d_1-f}. \tag{2}$$

Optics EXPRESS

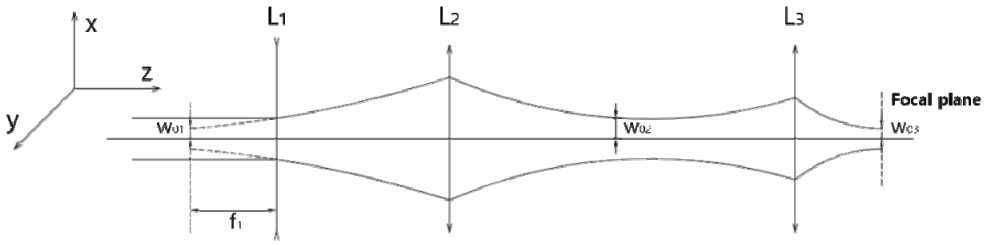

Fig. 4. Schematic of the transmission of a laser beam through the dynamic focusing system.

Equation (2) provides the position of the beam waist or focal point of the outgoing beam with respect to the lens. In other words, if a beam with beam waist at a distance d_1 away from the lens passes through the lens, it will converge at a distance d_2 on the other side of the lens. This result is consistent with the formula of the thin lens in ray optics. Next, we apply this equation for a real setup including the dynamic focusing system and objective lens to determine the relation between the lens L_1-lens L_2 distance and focus-objective lens distance. Figure 4 shows a schematic of the optical model of the dynamic focusing system. An incident collimated laser beam passes through the negative lens L_1 and diverges to the positive lens L_2 with a virtual focal position at a distance $|f_1|$ from the negative lens and beam waist w_{o1}. The outgoing beam from the dynamic focusing system is then focused at a distance q from the positive lens between positive lens L_2 and the objective lens with beam waist w_{o2}. The beam continuously passes through the objective lens and converges at a distance u with beam waist w_{o3}. The distance between the negative and positive lenses is denoted as h, and distance between the objective lens and the positive lens is ζ. The beam passing through the negative lens has a virtual beam waist at a distance $(h-f_1)$ from the positive lens ($f_1<0$). By applying Eq. (2), the distance q of the beam waist w_{o2} can be calculated as follows:

$$q=\frac{f_2(h-f_1)}{h-f_2-f_1}. \tag{3}$$

Accordingly, the distance between beam waist w_{o2} and the objective lens is $\zeta-q$, and the distance between the objective lens and positive lens is set as $\zeta=f+f_2$. The distance between beam waist w_{o3} and the objective lens is determined as follows:

$$\begin{aligned} u&=\frac{f(\zeta-q)}{\zeta-q-f}=f\frac{(f+f_2)(h-f_1-f_2)-f_2(h-f_1)}{f_2(h-f_1-f_2)-f_2(h-f_1)}=f\frac{f_2^2-f(h-f_1-f_2)}{f_2^2}, \\ h&=-\frac{f_2^2}{f^2}u+\frac{f_2^2}{f}+f_1+f_2. \end{aligned} \tag{4}$$

Equation (4) describes the relation between the positions of the negative lens and laser focus behind the objective lens. Furthermore, by applying Eq. (1), one can calculate the beam waists as follows:

$$w_{o1}^2+\left(\frac{\lambda f_1}{\pi w_{o1}}\right)^2=w_o^2, \tag{5}$$

Optics EXPRESS

$$w_{o1}^2+\left(\frac{\lambda(h-f_1)}{\pi w_{o1}}\right)^2=w_{o2}^2+\left(\frac{\lambda f_2(h-f_1)}{\pi w_{o2}(h-f_1-f_2)}\right)^2, \quad (6)$$

$$w_{o2}^2+\left(\frac{\lambda}{\pi w_{o2}}\left(f+f_2-\frac{f_2(h-f_1)}{h-f_2-f_1}\right)\right)^2=w_{o3}^2+\left(\frac{\lambda}{\pi w_{o3}}\left(f\frac{f_2^2-f(h-f_1-f_2)}{f_2^2}\right)\right)^2. \quad (7)$$

The irradiance of the laser beam at a specific point with beam radius w is given as follows:

$$I=\frac{c\varepsilon_o E_o^2}{\pi w^2}e^{-\frac{2(x^2+y^2)}{w^2}}. \quad (8)$$

where c is the speed of light, E_o is the amplitude of electric field of the wave, and (x, y, z) are the Cartesian coordinates of the point with the z-axis being the optical axis. Equation (8) indicates that the optical energy distribution at the focus mainly depends on the beam spot size in the experiment. We will examine the changes in beam spot size with respect to the position of the negative lens L_1 when the lens is moved around the initial position at which the beam propagating toward the objective lens is collimated.

3. Double-spot focus detection system using advanced image sensor

3.1 Description of double-spot focus detection system

The system detects the focal position of a laser beam in real time based on the configuration of beam spots produced by a double-hole mask on the image sensor with respect to the distance between the objective lens and target sample. From the beam-spot separation on the image sensor, the defocusing distance of the sample from laser focus can be precisely computed. The system includes a diode laser, the double-hole mask, a beam splitter, an objective lens, a target sample, a tube lens, and the image sensor. The laser beam passing through the double-hole mask is divided into two parallel beams. These beams pass through the objective lens, get reflected on the sample, pass through the objective lens and tube lens, and are finally incident on the image sensor, which is designed to accurately read the beam-spot separation. To fix the position of the image sensor, we conduct a calibration step. A sample (silicon wafer) is used to replace the target sample for the calibration step and to sketch the relation between the diode-laser beam-spot separation on the image sensor and the objective lens-sample distance that was presented in [30]. First, we block the diode laser beam from reaching the objective lens as well as the sample and control the position of the image sensor with a micro-positioning system until the two beam spots overlap. Second, the blocking plate is removed, and the sample is shifted by another micro-positioning system until the two beam spots on the image sensor overlap again; this position of the sample indicates the focal position of the laser beam. Third, because the image sensor cannot record the beam-spot separation when two beam spots start being overlapped, we shift the image sensor to a new position, where it can read the beam-spot spacing as the sample is positioned at the focus. This position of the sample is fixed, and the sample is replaced by the target sample.

Optics EXPRESS

3.2 Analytical model

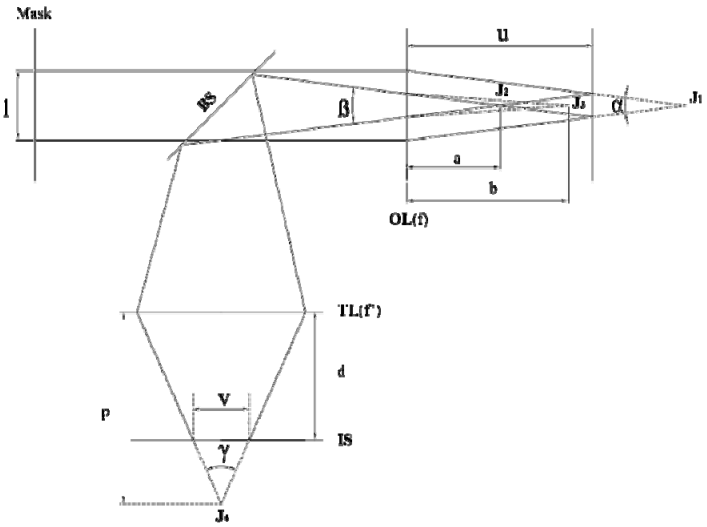

Fig. 5. Setup with only a double-hole panel.

Figure 5 shows the simplified optical setup of the focus detection system using an image sensor that reads the beam-spot separation, where f is the focal length of the objective lens, f' is the focal length of the tube lens, a is the distance between J_2 and the objective lens, b is the distance between J_3 and the objective lens, c is the distance from the focusing point of fractional laser beams to the tube lens, d is the distance between the tube lens and image sensor, ρ is the image sensor-beam splitter-objective lens distance, l is the hole spacing on the mask, α is the angle made by fractional laser beams after the first transmission through the objective lens, β is the angle made by fractional laser beams after the second transmission through the objective lens (reflected beam), and γ is the angle made by fractional laser beams after a single transmission. According to Fig. 5, the intersections at point J_2 and at point J_1 are symmetric over the sample as a perfect mirror. Thus, we express the distance between J_2 and the objective lens as follows:

$$a = 2u - f. \tag{9}$$

Subsequently, the intersection at point J_3 is regarded as the image of the intersection at point J_2 through the objective lens OL. The position of J_3 with respect to the objective lens is depicted by b :

$$b = \frac{(2u - f)f}{2(f - u)}. \tag{10}$$

The intersection at point J_4 is regarded as the image of the intersection at point J_3 through the tube lens TL with the distance $(\rho - d)$ between the tube lens and objective lens, and we have the position of J_3 with respect to the tube lens as $(\rho - d - b)$. Accordingly, the distance from the focusing point of beams to the tube lens, p is computed based on the relation between the image and object through the tube lens:

Optics EXPRESS

$$p = \frac{(\rho - d - b) f'}{\rho - d - f' - b} = \frac{\left(\rho - d - \frac{(2u - f) f}{2(u - f)}\right) f'}{\rho - d - f' - \frac{(2u - f) f}{2(u - f)}}. \tag{11}$$

The relations between α and β and between γ and β are expressed as follows:

$$\frac{\tan\left(\frac{\beta}{2}\right)}{\tan\left(\frac{\alpha}{2}\right)} = \frac{a}{b} = \frac{2(f - u)}{f}, \tag{12}$$

$$\frac{\tan\left(\frac{\gamma}{2}\right)}{\tan\left(\frac{\beta}{2}\right)} = \frac{\rho - d - b}{p} = \frac{2(\rho - d - f')(u - f) - (2u - f) f}{2(u - f) f'}. \tag{13}$$

By multiplying (12) and (13) side by side, we obtain

$$\tan\left(\frac{\gamma}{2}\right) = -\frac{2(\rho - d - f')(u - f) - (2u - f) f}{f' f} \tan\left(\frac{\alpha}{2}\right). \tag{14}$$

Equation (14) describes the linear relation between the beam-spot separation on the image sensor and the objective lens-sample distance. The relation between the beam-spot separation on the image sensor v and the objective lens-target sample distance u is given with $\tan\left(\frac{\alpha}{2}\right) = \frac{l}{2f}$ as follows:

$$v = 2(p - d)\tan\left(\frac{\gamma}{2}\right) = -\frac{\left[2u\left(d^2 - (\rho - f)d + \rho f' - ff'\right) - 2fd^2 + 2f\rho d - 2ff'\rho - f^2 d + f^2 f'\right] l}{f^2 f'}. \tag{15}$$

Based on this equation, a computer can determine the defocusing distance of the sample and control the micro-positioning system to precisely shift the focal position. The linearity of the equation is evident in Fig. 6, which shows the dependence of beam-spot spacing on the target sample's position along the optical axis as well as images of beam spots on the image sensor when the sample is located at the focus (marked by red circle) and defocus positions. As described in the calibration step, when the sample is positioned at the focus, the two beam spots are not overlapped so that the image sensor can record the spacing between them. Along with the variation in beam-spot separation, the figure also indicates the diameter of drilled holes made by the fabrication laser on the target surface with respect to the target sample's position.

Optics EXPRESS

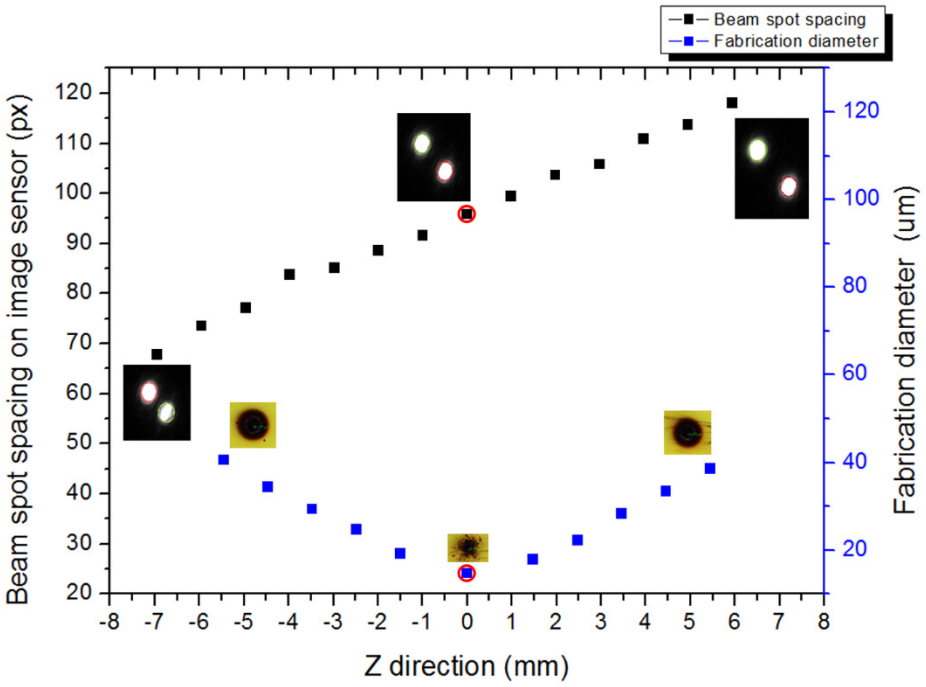

Fig. 6. Fabrication diameter and variation in beam-spot separation with respect to the target sample's position along the optical axis [30].

4. Combination of dynamic focusing and focus detection systems

4.1 Principle

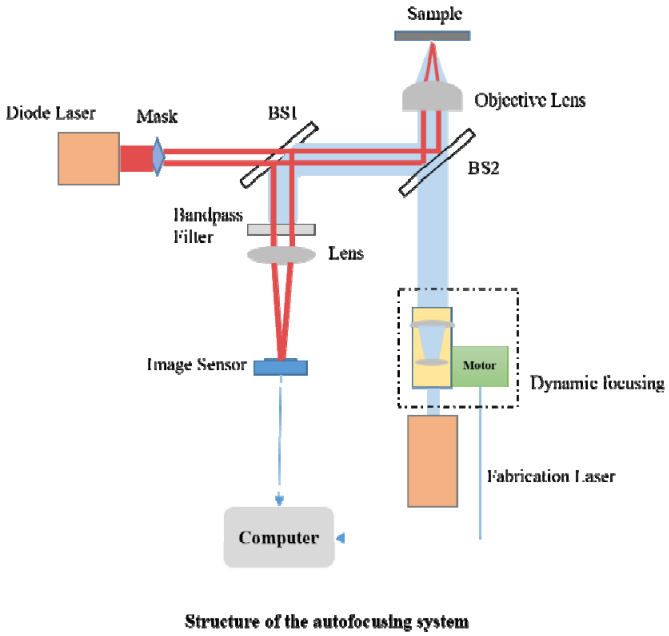

Fig. 7. Schematic of the combination of dynamic focusing and focus detection systems.

Optics EXPRESS

An automatic laser focus controlling system is required to locate the focal point of laser beam on the target sample, wherever the sample is positioned. To fulfill this purpose, a combination of dynamic focusing and focus detection systems is designed. The design of the system is illustrated in the Fig. 7. The integrated system includes the dynamic focusing system (one fixed positive lens and one movable negative lens), the objective lens, the double-hole mask, the bandpass filter, the tube lens, the image sensor, the target sample, a diode laser, and a high-power fabrication laser. The diode laser beam is directed through the focus detection system and is eventually incident on the image sensor to give information on the beam-spot configuration, while the fabrication beam is directed through the dynamic focusing system to the target sample, reflected to the bandpass filter, and finally absorbed by this device. The focus detection system identifies the defocusing distance as well as the position of the target surface on the basis of beam spot size when the sample is at the focus and the linear relation between the diode-laser beam-spot spacing on the image sensor and the objective lens-sample distance. Simultaneously, the dynamic focusing system positions the laser focus on the surface. This can be performed by finding the intersection between relations (4) and (15) when the two relations are sketched on the same plane; this computation is performed using the optical simulation software Zemax. In Eq. (4), u is defined as the distance between the objective lens and laser focus, which is consistent with the objective lens-target sample distance defined in Eq. (15). From this combination, the computer can automatically control the position of the negative lens inside the dynamic focusing system to locate the laser focus on the target surface during laser processing.

4.2 Experiment and analysis

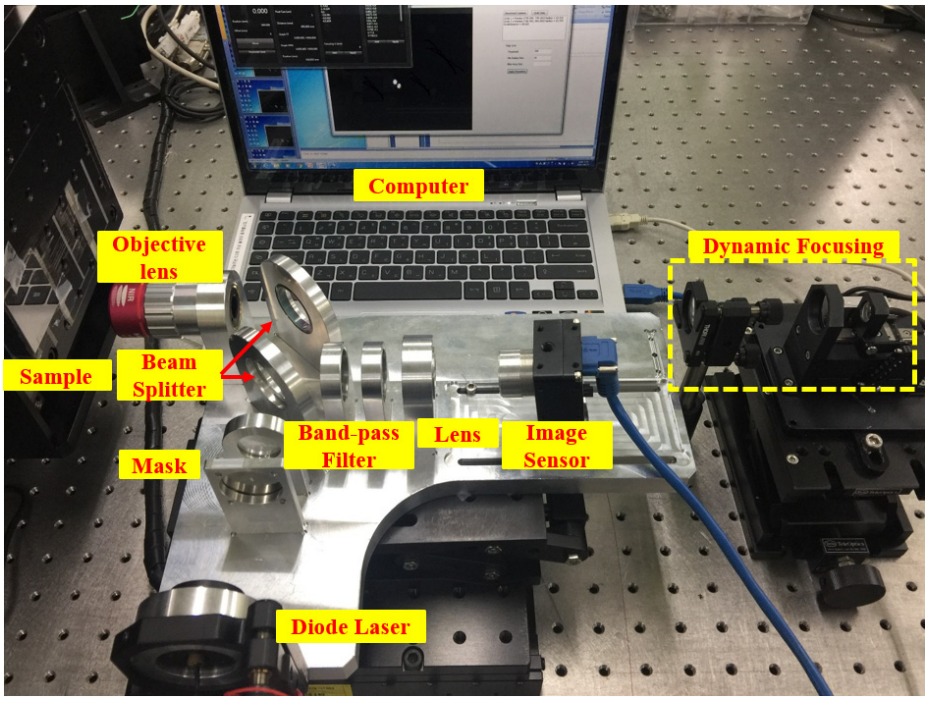

Fig. 8. Experimental setup.

The complete optical setup for automatic real-time focus control is shown in Fig. 8. In this setup, we employ a nanosecond laser (G4, 50 W; beam diameter of ~3 mm, wavelength of 1064 nm, pulse duration of 5 ns, M^2 = 1.3, random polarization, SPI Lasers Ltd, Southampton, United Kingdom) for laser micromachining, a diode laser with a wavelength of 655 nm for focus determination, an objective lens (M Plan Apo NIR 5x, Mitutoyo, Japan)

Optics EXPRESS

with a focal length of 40 mm, a tube lens, a sample (silicon wafer), a double-hole mask described in [30], a bandpass filter (FB780-10, CWL = 780 nm, FWHM = 10 nm, Thorlabs) that blocks the fabrication laser and allows the diode laser to pass through, an image sensor named u-Nova20M (1600 × 1200, 50 fps, Mono, Global Shutter, CMOS) with a high response speed that can precisely and rapidly record the beam-spot spacing based on intensity peaks as well as the beam spot size within 0.02 s [30], several beam splitters, and a dynamic focusing system including a movable negative lens L_1 with a focal length of −50 mm and a fixed positive lens L_2 with a focal length of 100 mm. In this dynamic system, the two lenses are initially at a separation of 50 mm, and the distance between lens L_2 and the objective lens is 140 mm. The target sample and lens L_1 are automatically movable by micro-positioning panels or motors that are all connected to the computer.

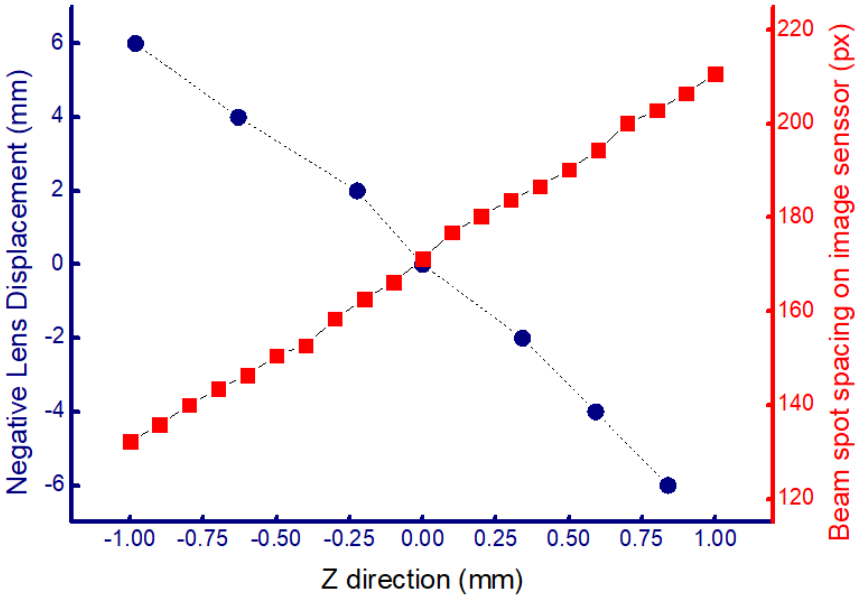

Fig. 9. Experimental relations between beam-spot separation and objective lens-sample distance and between dynamic focusing lenses' separation and objective lens-sample distance.

The experimental relations between the diode-laser beam-spot separation and objective lens-sample distance and between the lens L_1-lens L_2 separation and the objective lens-sample distance are obtained on the same plane in Fig. 9 through calibration steps [30] in focus detection and the movement of negative lens L_1 around the initial point, as described in the section 2.1. The theoretical absolute slope of the relation between beam-spot separation and objective lens-sample distance is $\left(\frac{2(d^2-(\rho-f)d)l}{f^2f'}+\frac{2(\rho-f)l}{f^2}\right)$ from (15), and that of the relation between lens L_1-lens L_2 separation and the objective lens-sample distance is $\frac{f_2^2}{f^2}$ from (4). In this figure, the vertical axis on the left indicates the position of lens L_1, while the vertical axis on the right indicates the beam-spot spacing on the image sensor. The horizontal axis indicates the distance between the objective lens and sample on the optical axis (Z-direction). The intersection of the two relations is acquired by plotting the two graphs on the same scale, and this intersection refers to the position of the sample surface for adjusting the laser focus by automatically shifting the negative lens via a motor controlled by the computer. In Fig. 9, the acquired focal position is marked as point 0 on the z-axis, which can be

Optics EXPRESS

recognized by the computer. The linearity of the obtained relations demonstrates the consistency between theory and experiment with approximately equal absolute slopes. According to Table 1, the conservation of beam spot size maintains the optical energy distribution at the focal position based on Eq. (8) and thereby guarantees that the micro-pattern size does not change considerably when the sample is slightly shifted to alter the working distance (or around the focal position). The general operation of the focus detection system is indicated in Visualization 1. The method is superior to previous methods because it allows for the flexible movement of the laser focal point and real-time detection of this point based on the configuration of reflected diode laser beam spots with the support of a motor and micro-positioning panel. Furthermore, the fact that a computer precisely explores the intersection of linear relations contributes to the precision of the technique.

5. Conclusion

We proposed an automatic real-time focus control system based on the concepts of in situ real-time focus detection using an advanced image sensor and dynamic focusing. The dynamic focusing system plays a role of shifting the laser focus, and the focus detection system explores the focal position of the laser beam and defocusing distance. This focus inspection system integrates the dynamic focusing system and target sample movements. The method employs the linear relation between beam-spot spacing on the image sensor created by a double-hole mask and the distance between the objective lens and sample as well as the laser focus controlled via the dynamic focusing system utilizing one negative lens and one positive lens. The linear relations between the beam-spot separation and objective lens-sample distance as well as between the lens L_1-lens L_2 separation and objective lens-sample distance intersect each other at one point, which is the proper focal position at which the fabrication energy is the most intense. The results of a direct experiment and Zemax simulation illustrate the consistency between the analytical formula and practical sketches. The small deviation (0.1%) in focal spot size when the negative lens is shifted around the zero position demonstrates that the system maintains the fabrication size and energy distribution on the target sample surface during the focus detection. Furthermore, the focus control is manipulated by computer programming, which allows for high reproducibility, accuracy, and versatility in industrial applications, such as micro-groove fabrication on stepped surfaces and optical microscope technology.

Funding

Korean-government-funded Research Project NK202B (the main research project of the Korea Institute of Machinery and Materials) and R0004727 (the research project of economic cooperation and industry promotion “Development of the Low Cost, Low Power Near infrared Laser Pulse Illuminator and Night Vision System”).